Available online at www.sciencedirect.com
ScienceDirect
Journal of Computational Physics 227 (2008) 4486–4498
JOURNAL OF COMPUTATIONAL PHYSICS
www.elsevier.com/locate/jcp

An immersed boundary–lattice-Boltzmann method for the simulation of the flow past an impulsively started cylinder

Alexandre Dupuis, Philippe Chatelain, Petros Koumoutsakos *

Computational Science, ETH Zurich, CH-8092 Zurich, Switzerland

Received 18 March 2007; received in revised form 11 December 2007; accepted 9 January 2008
Available online 20 January 2008

Abstract

We present a lattice-Boltzmann method coupled with an immersed boundary technique for the simulation of bluff body flows. The lattice-Boltzmann method for the modeling of the Navier–Stokes equations, is enhanced by a forcing term to account for the no-slip boundary condition on a non-grid conforming boundary. We investigate two alternatives of coupling the boundary forcing term with the grid nodes, namely the direct and the interpolated forcing techniques. The present LB–IB methods are validated in simulations of the incompressible flow past an impulsively started cylinder at low and moderate Reynolds numbers. We present diagnostics such as the near wall vorticity field and the drag coefficient and comparisons with previous computational and experimental works and assess the advantages and drawbacks of the two techniques.

Keywords: Immersed boundary; Lattice-Boltzmann; Impulsively started cylinder; Bluff body flows

1. Introduction

A number of important flow phenomena in science and engineering, ranging for example from hemodynamics [3] and fish swimming [35] to robotic insects [11] and prosthetic heart valves [29], involve flows past complex geometries. The computational study of these flows requires the development of numerical techniques capable of handling complex unsteady geometries. A number of computational methods, such as finite elements, finite volume and unstructured mesh finite differences (see [23, and references therein]) have been developed that can handle complex geometries for systems such as blood flow past endovascular devices [5] or multiphase turbulent flows in realistic combustors [26]. More recently, lattice-Boltzmann methods [34] have been advocated as effective computational tools for the simulation of complex flows ranging from car aerodynamics to flows in porous media. The results of these simulations may depend however on the grid distribution

* Corresponding author. Tel.: +41 1 632 5258; fax: +41 1 632 1703.
E-mail address: petros@ethz.ch (P. Koumoutsakos).

0021-9991/$ - see front matter © 2008 Elsevier Inc. All rights reserved.
doi:10.1016/j.jcp.2008.01.009

[31,18], while intensive meshing requirements may adversely affect the efficiency of the simulations for flows with time dependent, complex geometries. In the early 1970s motivated by problems in biological flows, Peskin [28,30] pioneered the use of immersed boundary methods that require a cartesian grid and a suitable modification of the governing equations to take into account the effects of the boundaries. The simplicity in meshing and the relative ease of implementation of these techniques has led to intensive research efforts (see [24, and references therein]) making the IB technique a potent alternative for simulations of flows with complex, unsteady geometries.

In this work, we present the coupling of immersed boundary (IB) and lattice-Boltzmann (LB) methods. LB models [34] solve the Navier–Stokes equations of incompressible fluids by following the evolution of distribution functions on a lattice. Boundaries are approximated on the regular lattice in a staircase fashion making them suitable for simulations of flows past grid conforming geometries. The accuracy of the method depends on the detail of the boundary representation and efficiency requirements dictate the local refinement of the lattice [12]. A number of works have addressed the coupling of IB and LB methods. Feng and Michaelides [14,15] report on continuous and discrete forcing models applied to sedimentation problems. Peng et al. [27] couple a discrete forcing model to a multi-relaxation time LB model considering variable resolution. Shi and Phan-Tien [32] propose a model that integrates distributed Lagrange multipliers and fictitious domain methods in the framework of LB models. In this paper, we present an alternative model coupling an LB model of the incompressible Navier–Stokes equations with an IB technique. The algorithmic novelty of our work consists of the simple way in which the LB model incorporates the IB forcing term. In addition, we investigate two variants of coupling the boundary force with the Eulerian grid namely: a direct forcing (DF) and an interpolated forcing (IF) distinguished by the way in which the forcing term from the boundary is computed on the grid nodes.

The present method is validated on simulations of the flow past an impulsively started circular cylinder at moderate Reynolds numbers. The flow past an impulsively started cylinder is a well-established benchmark problem and the subject of detailed experimental investigations for Reynolds numbers ranging from 40 to 10,000 [9,10,4]. The simulation of this flow is challenging as it requires the accurate tracking of the initial sharp vorticity generation on the cylinder surface and the precise identification of the subsequent regions of the disruption of the primarily shedded vortices by their induced secondary vortical fields. There is a plethora of results from simulations using different numerical methods such as finite difference schemes [8,2], vortex methods [20], wavelet collocation schemes [19], and lattice-Boltzmann models [22]. In these simulations, diagnostics such as streamlines, vorticity contours and in particular the drag coefficient have been used to elucidate the advantages and drawbacks of the different methodologies. We present such diagnostics and use the value of the asymptotic drag coefficient to establish the order of accuracy of our method.

The paper is organized as follows: we first present in Section 2 the hybrid scheme and discuss the LB model and the two variants of the IB algorithm. In Section 3, we present simulations of the flow around an impulsively started cylinder at low and moderate Reynolds numbers. We quantify the convergence of both IB approaches and conclude in Section 4.

2. The model

2.1. Lattice-Boltzmann (LB) model

We consider viscous incompressible flows described by the velocity–pressure formulation of the Navier–Stokes equations

$$\frac{\partial \mathbf{u}}{\partial t} + (\mathbf{u}\cdot\nabla)\mathbf{u} = -\nabla p/\rho + \nu\nabla^2\mathbf{u} + \mathbf{g} \tag{1}$$

$$\nabla\cdot\mathbf{u} = 0 \tag{2}$$

where $\mathbf{u}$ the velocity, p the pressure, ρ the density of the fluid. The forcing term $\mathbf{g}$ accounts for the no-slip condition at the boundary and it is introduced to enable the use of the immersed boundary technique presented below.

We solve the equations of motion (1) and (2) using a lattice-Boltzmann algorithm [34]. The LB model entails the evolution of particle distribution functions f_i on a d-dimensional regular lattice with z links at each lattice point $\mathbf{r}$. The label i denotes velocity directions and runs between 0 and z. $DdQz+1$ is a standard lattice topology classification. The $D2Q9$ lattice we use here has the following velocity vectors $\mathbf{v}_0=(0,0)$, $\mathbf{v}_i=(\cos((i-1)\pi/2),\sin((i-1)\pi/2))$ for $i=1$–4, and $\mathbf{v}_i=(\cos((i-5)\pi/2+\pi/4),\sin((i-5)\pi/2+\pi/4))$ for $i=5-8$ in lattice units.

The lattice-Boltzmann dynamics are given by

$$f_i(\mathbf{r}+\Delta t\mathbf{v}_i,t+\Delta t)=f_i(\mathbf{r},t)+\frac{1}{\tau}(f_i^{\mathrm{eq}}(\mathbf{r},t)-f_i(\mathbf{r},t))+\Delta t\frac{w_i\rho}{c_s^2}\mathbf{v}_i\cdot\mathbf{g} \tag{3}$$

where Δt is the time step of the simulation, τ the relaxation time, $c_s=1/\sqrt{3}$ is the speed of sound and w_i are weights chosen as $w_0=4/9$, $w_i=1/9$ for $i=1-4$ and $w_i=1/36$ for $i=5-8$. The equilibrium distribution function f_i^{eq} is a function of the density ρ and the fluid velocity $\mathbf{u}$ defined as

$$\rho=\sum_{i=0}^{z}f_i,\quad \rho\mathbf{u}=\sum_{i=0}^{z}f_i\mathbf{v}_i \tag{4}$$

The equilibrium distribution function is chosen as

$$f_i^{\mathrm{eq}}(\mathbf{r},t)=w_i\rho\left(1+\frac{\mathbf{v}_i\cdot\mathbf{u}}{c_s^2}+\frac{(\mathbf{v}_i\cdot\mathbf{u})^2}{2c_s^4}-\frac{\mathbf{u}^2}{2c_s^2}\right) \tag{5}$$

We have also performed simulations using an alternative forcing term as described by Guo et al. [16]. Guo's model eliminates explicitly non-negligible spurious temporal and spatial terms. The present results do not indicate any significant differences between the two approaches.

Performing a Chapman–Enskog expansion on the LB dynamics [7] shows, in the low Mach number limit, that Eqs. (1) and (2) are recovered with a kinematic viscosity expressed as

$$\nu=\frac{(\Delta r)^2}{\Delta t}\frac{1}{3}\left(\tau-\frac{1}{2}\right) \tag{6}$$

where the Mach number is defined as $Ma=U/c_s$ with U being the characteristic velocity of the system, and Δr is the lattice spacing.

2.2. Immersed boundary (IB) methods

In immersed boundary methods the presence of the boundary is accounted by adding a forcing term on the governing flow equations [28,30]. The forcing term is computed so as to enforce the no-slip boundary condition on the surface of the body. The equations are usually discretized on an Eulerian grid which does not need to coincide with the location of the body and a forcing term has to be computed on the grid nodes. In the present work, we follow the technique originally proposed by Mohd-Yusof [25] to determine the forcing term that is required to impose a desired velocity $\mathbf{u}^d$ at the boundary.

The governing equation (1) is rewritten as

$$\frac{\partial\mathbf{u}}{\partial t}=\frac{\mathbf{u}^*(\mathbf{r},t+\Delta t)-\mathbf{u}(\mathbf{r},t)}{\Delta t}=-(\mathbf{u}\cdot\nabla)\mathbf{u}-\nabla p+\nu\nabla^2\mathbf{u}=\mathrm{RHS} \tag{7}$$

where $\mathbf{u}^*$ is the velocity at time $t+\Delta t$ with no forcing term considered. Including a forcing term leads to

$$\frac{\mathbf{u}^d(\mathbf{r},t+\Delta t)-\mathbf{u}(\mathbf{r},t)}{\Delta t}=\mathrm{RHS}+\mathbf{g}(\mathbf{r},t) \tag{8}$$

where $\mathbf{u}^d$ is the desired velocity. Subtracting Eq. (7) from (8) leads to an expression for the forcing term

$$\mathbf{g}(\mathbf{r},t)=\frac{\mathbf{u}^d(\mathbf{r},t+\Delta t)-\mathbf{u}^*(\mathbf{r},t+\Delta t)}{\Delta t} \tag{9}$$

This methodology differs from existing boundary enforcement schemes in several aspects. The LB–IB method of Feng and Michaelides [14,15] relies on the explicit computation of $\mathbf{g}$ from Eq. (1). The present approach, follows the works of Mohd-Yusof [25] and Fadlun et al. [13], and evaluates $\mathbf{g}$ by advancing to the solution $\mathbf{u}^*(\mathbf{r},t+\Delta t)$. This preliminary step can be treated in a very efficient manner thanks to two properties of the LB method:

1. LB simulates a compressible flow so that the velocities $\mathbf{u}^*$ only need computation in a neighborhood of the boundaries.
2. This step involves only the streaming part of the LB model as the relaxation to the equilibrium distribution (the second term of the right-hand side of Eq. (3)) does not change the velocity ($\rho\mathbf{u} = \sum f_i^{\mathrm{eq}}\mathbf{v}_i$, see [7] for details).

Other flexible boundary schemes in LB methods include the volumetric bounce back of Chen et al. [6] which Li et al. [22] recently applied to the flow past an impulsively started cylinder. The complexity of the volumetric bounce back is arguably higher, than the present LB–IB approach, as it involves more accounting and the explicit discretization of the boundary into facets. The present approach allows implicit boundary representations in its IF variant (see below).

The coupling of LB and IB requires a procedure to enable the communication of the effect of the body force between the Eulerian grids and the surface of the body. In the present paper, we investigate two variants: a direct forcing (DF) and an interpolated forcing (IF) approach. The DF aims at distributing, on the lattice, forces known along the boundary from Eq. (9). In turn, the IF determines velocities at lattice nodes close to the boundary by using a second-order interpolation scheme and by applying accordingly a forcing term. In the following we use lower-case and upper-case variables to represent value defined on the Eulerian lattice and on the Lagrangian boundary, respectively.

2.2.1. Direct forcing approach (DF)

In the DF, velocity boundary conditions $\mathbf{U}^d$ are enforced on the boundary by determining a Lagrangian forcing term which is subsequently distributed on the lattice. This is done by first performing an streaming step to determine $\mathbf{u}^*$ corresponding to the flow field without a forcing term. We then use a discretization of delta function [28] to determine velocities along the boundary as

$$\mathbf{U}^*(s,t) = \sum_{\mathbf{r}} \mathbf{u}^*(\mathbf{r},t)\delta_h(\mathbf{r}-\mathbf{R}(s,t)) \tag{10}$$

where s is the boundary coordinate, $\mathbf{R}(s,t)$ the boundary position and $\delta_h(\mathbf{r}-\mathbf{R}(s,t)) = \Pi_\alpha\delta(r_\alpha - R_\alpha(s,t))$ is the discrete delta function and α runs over the Cartesian coordinates. The discrete delta function is defined as

$$\delta_h(x) = \begin{cases} \frac{1}{4\Delta r}\left(1+\cos\left(\frac{\pi|x|}{2\Delta r}\right)\right), & \text{if} \quad |x| \leqslant 2\Delta r \\ 0, & \text{otherwise} \end{cases} \tag{11}$$

The Lagrangian body force $\mathbf{G}(s,t)$ is found by using Eq. (9) and is in turn distributed on the lattice by applying the same delta function δ_h. This leads to an Eulerian forcing term

$$\mathbf{g}(\mathbf{r},t) = \sum_{s} \mathbf{G}(s,t)\delta_h(\mathbf{r}-\mathbf{R}(s,t)) \tag{12}$$

We note that distributing a Lagrangian force $\mathbf{G}$ using Eq. (12) implies that the desired velocity $\mathbf{U}^d$ is not *exactly* enforced at the boundary. However, as we shall see below, the discrepancy reduces as the resolution increases.

2.2.2. Interpolating force approach (IF)

Following the work of Fadlun et al. [13], the IF determines forces $\mathbf{g}_1$ in the direct vicinity of the boundary so as to enforce velocities $\mathbf{u}_1^d$ via a bilinear interpolation scheme. The lattice nodes and the boundary points

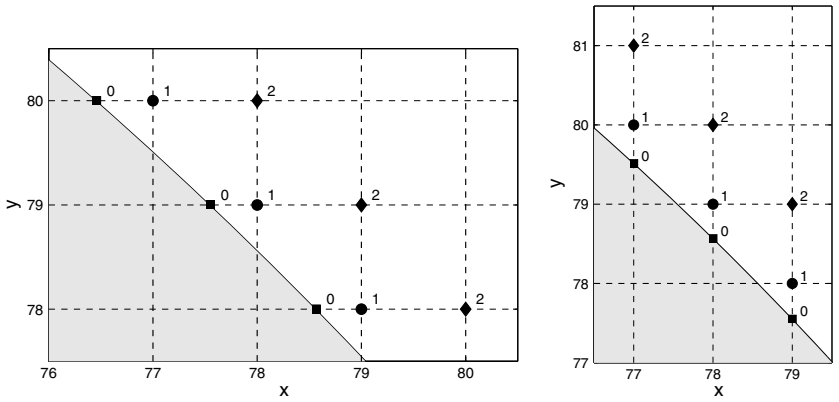

Fig. 1. Lattice nodes and boundary points involved in the interpolation procedure of (left) the x-component and (right) the y-component of the velocity $\mathbf{v}_1$. Gray areas are the insides of the object defined by the boundary. Coordinates are expressed in simulation units.

involved in the interpolation procedure are depicted in Fig. 1. Velocities in the direct vicinity of the boundary are computed as

$$\mathbf{u}_1^d = \frac{\mathbf{U}_0^d + \mathbf{d}\cdot\mathbf{u}_2^*}{1+\mathbf{d}} \tag{13}$$

where subscripts denote locations (see Fig. 1), $\mathbf{d}$ is the distance between lattice node 1 to boundary point 0.

3. Results

We apply the method to the simulation of viscous incompressible flows past an impulsively started cylinder at moderate Reynolds numbers and investigate the convergence of the method.

3.1. Flow past an impulsively started cylinder

The flow past an impulsively started cylinder is initialized with the corresponding irrotational flow past a cylinder of diameter D with speed u_0 at infinity [1]. The velocity components are expressed in polar coordinates as

$$u_r = u_0\left(1-\frac{D^2}{4r^2}\right)\cos\theta, \quad u_\theta = -u_0\left(1+\frac{D^2}{4r^2}\right)\sin\theta \tag{14}$$

The velocity components in Cartesian coordinates reads

$$u_x = u_r\cos\theta - u_\theta\sin\theta, \quad u_y = u_r\sin\theta + u_\theta\cos\theta \tag{15}$$

The distribution functions f_i are initialized following a procedure detailed in [7,21]. We consider the Chapman–Enskog expansion of the functions f_i in power series of a small parameter ϵ as $f_i = f_i^{(0)} + \epsilon f_i^{(1)} + \cdots$. It is shown that the zeroth-order is the equilibrium distribution function as described in Eq. (5) and that the first-order is related to velocity gradients as [7]

$$\epsilon f_i^{(1)} = -\frac{w_i\tau}{c_s^2}\sum_{\alpha\beta} Q_{i\alpha\beta}\partial_\alpha(\rho u_\beta) \tag{16}$$

where $Q_{i\alpha\beta} = v_{i\alpha}v_{i\beta} - c_s^2\delta_{\alpha\beta}$ with $\delta_{\alpha\beta}$ being the Kronecker symbol.

The hydrodynamics of an incompressible fluid being well approximated by the zeroth and first-order of the expansion [7], we use Eqs. (5) and (16) to determine the initial distribution functions according to Eq. (15). The initial distribution functions are

$$
\begin{aligned}
f_0(\mathbf{r},t) &= f_0^{\mathrm{eq}}(\mathbf{r},t) + w_0\tau(S_{xx}+S_{yy})\\
f_1(\mathbf{r},t) &= f_1^{\mathrm{eq}}(\mathbf{r},t) + w_1\tau(-2S_{xx}+S_{yy})\\
f_2(\mathbf{r},t) &= f_2^{\mathrm{eq}}(\mathbf{r},t) + w_2\tau(-2S_{yy}+S_{xx})\\
f_3(\mathbf{r},t) &= f_3^{\mathrm{eq}}(\mathbf{r},t) + w_3\tau(-2S_{xx}+S_{yy})\\
f_4(\mathbf{r},t) &= f_4^{\mathrm{eq}}(\mathbf{r},t) + w_4\tau(-2S_{yy}+S_{xx})\\
f_5(\mathbf{r},t) &= f_5^{\mathrm{eq}}(\mathbf{r},t) + 2w_5\tau(-S_{xx}-S_{yy}-3S_{xy})\\
f_6(\mathbf{r},t) &= f_6^{\mathrm{eq}}(\mathbf{r},t) + 2w_6\tau(-S_{xx}-S_{yy}+3S_{xy})\\
f_7(\mathbf{r},t) &= f_7^{\mathrm{eq}}(\mathbf{r},t) + 2w_7\tau(-S_{xx}-S_{yy}-3S_{xy})\\
f_8(\mathbf{r},t) &= f_8^{\mathrm{eq}}(\mathbf{r},t) + 2w_8\tau(-S_{xx}-S_{yy}+3S_{xy})
\end{aligned}
\tag{17}
$$

where $S_{\alpha\beta} = (\partial_\alpha(\rho u_\beta) + \partial_\beta(\rho u_\alpha))/2$ is the strain rate tensor. Derivatives of the velocity are evaluated with a second-order finite difference scheme.

We use the following boundary conditions on the velocity field. A Dirichlet condition is imposed at the inlet, setting $(u_x,u_y)(0,y) = (u_0,0)$. At the outlet we impose a first-order accurate homogeneous Neumann condition $(u_x,u_y)(L_x,y) = (u_x,u_y)(L_x-1,y)$. Periodic conditions are used in the y-direction. As for the initial conditions, these boundary conditions are translated in terms of the distribution functions, this time using one-sided finite differences for the strain rates. We note that this procedure requires the prior computation of the inlet and outlet densities. Using Eq. (4), they are recovered from the boundary conditions and the outgoing side of the distributions

$$
\rho_{\mathrm{inlet}} = \frac{(f_0+f_2+f_4)+2(f_3+f_6+f_7)}{1-u_x}, \quad \rho_{\mathrm{outlet}} = \frac{(f_0+f_2+f_4)+2(f_1+f_5+f_8)}{1+u_x} \tag{18}
$$

3.2. Flow at a low Reynolds number Re = 40

We first consider the flow past an impulsively started cylinder at a low Reynolds number $Re = 40$. The cylinder has a diameter $D = 20$ and is centered within a domain $100D \times 100D$. This domain size is chosen to reduce artifacts due to boundary conditions and to coincide with the geometry proposed in Li et al. [22]. Fig. 2 shows the velocity on the flow axis downstream of the cylinder at various times $T = 2Ut/D$. We observe a close match between the results obtained with the IF and Li's results at all times. Simulation results obtained with the DF differ slightly from the ones obtained with the IF with a discrepancy that is growing in time. Fig. 2 displays the maximum $e_{\max}$ and mean $\langle e\rangle$ error defined as

$$
e_{\max} = \max\frac{|u_x^{\mathrm{DF}}(\mathbf{x}) - u_x^{\mathrm{IF}}(\mathbf{x})|}{u_0} \quad \text{and} \quad \langle e\rangle = \frac{\langle |u_x^{\mathrm{DF}}(\mathbf{x}) - u_x^{\mathrm{IF}}(\mathbf{x})|\rangle}{u_0} \tag{19}
$$

where $\mathbf{x}$ is a downstream location along the flow axis and $\langle\,\rangle$ denotes a spatial average.

Fig. 3 shows the evolution of the recirculation length L on the flow axis and of the drag coefficient $C_{\mathrm{D}} = -2F/D/u_0^2$, where F is the force acting on the cylinder. There is agreement between the present simulation results and the results from Li et al. [22] and Koumoutsakos and Leonard [20]. We observe that the recirculation length is overestimated when using the DF. This can be attributed to the mollification of the Dirac delta function in the DF scheme which in a sense increases the effective diameter of the body. In contrast IF does not rely on the mollification of the interface. We note that while the present resolution is relatively coarse when compared to the one presented in Ref. [22] we obtain comparable results.

To quantify the convergence of the present IB–LB method, we measure the error associated to a given resolution when computing the drag coefficient around an impulsively started cylinder centered within a domain of size $30D \times 20D$. The error associated to a given resolution Δx is defined as the difference between the averaged value to the one obtained when considering the finest resolution. The boundary conditions are the same as above. The drag coefficients computed considering the finest resolution, being 160 lattice nodes across the cylinder, are $C_{\mathrm{D}}^{\mathrm{DF}} = 1.6285$ and $C_{\mathrm{D}}^{\mathrm{IF}} = 1.6159$. The evolution of the drag coefficient is monitored until $T = 50$ and an averaged value is measured between $T = 45$ and $T = 50$. Fig. 4 shows the convergence of the error

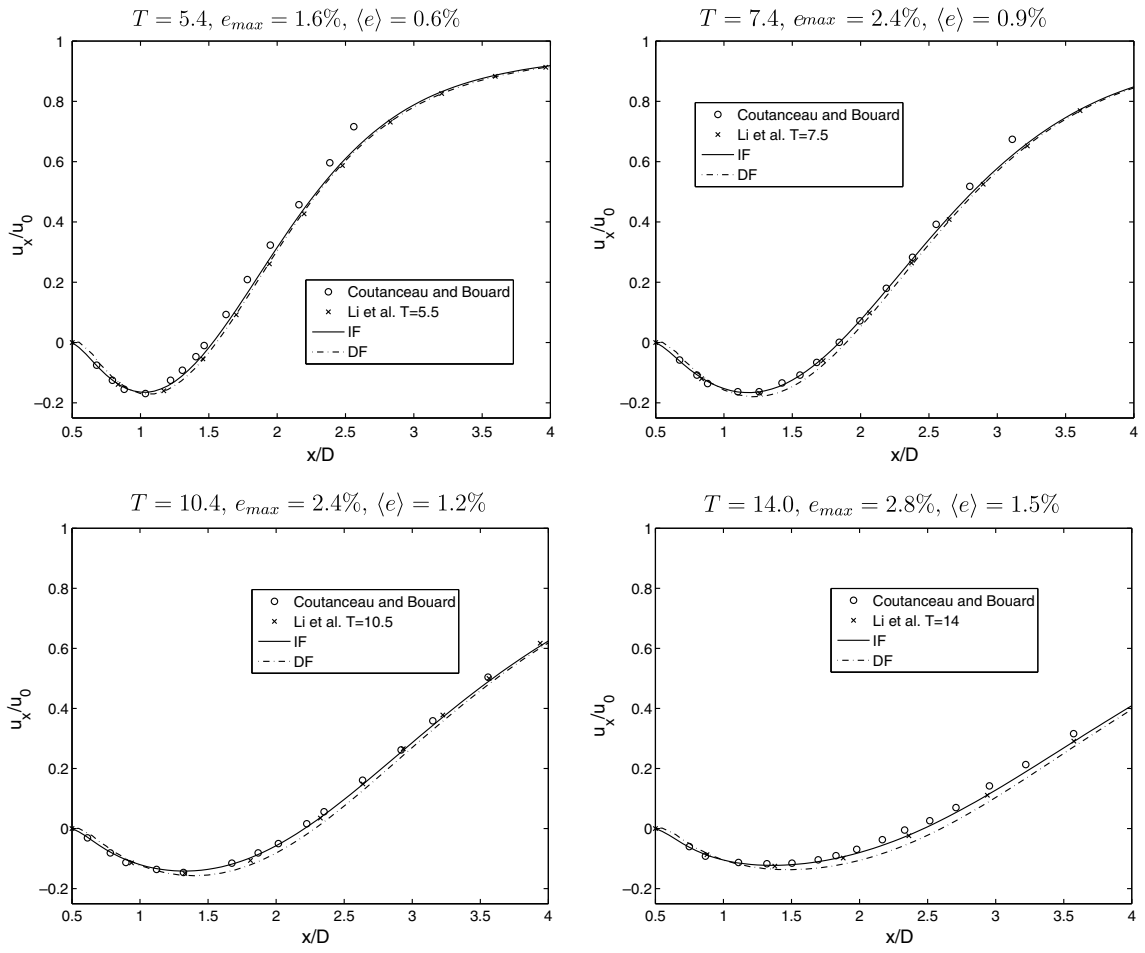

Fig. 2. Distributions of the x-velocity on the flow axis behind an impulsively started cylinder at $Re = 40$ and at different times T. Present simulation results using the IF (solid line) and DF (dashed line) are compared to experiments by Coutanceau and Bouard [9,10] (circle) and LB simulations by Li et al. [22] (cross).

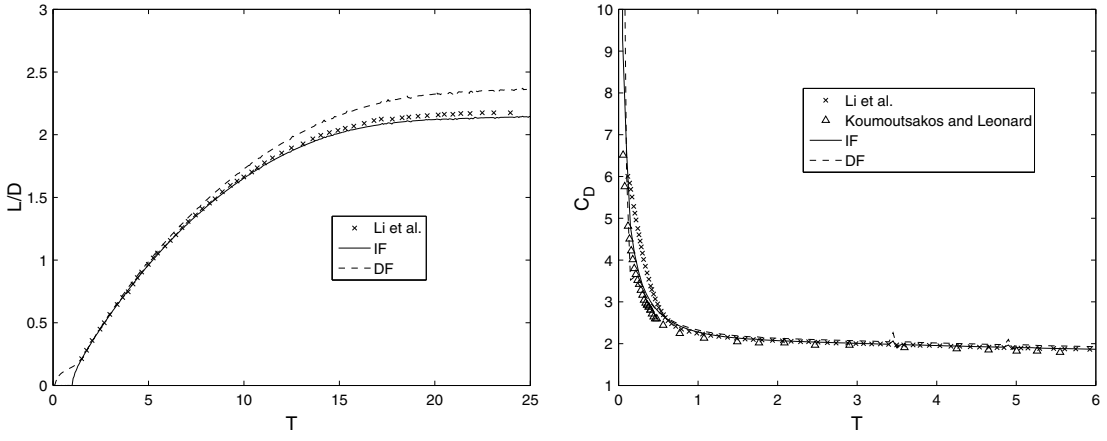

Fig. 3. Evolution of (left) recirculation length on the flow axis and of (right) the drag coefficient at $Re = 40$. Simulations results using IF (solid line) and DF (dashed line) are compared to results from Li et al. [22] (cross) and Koumoutsakos and Leonard [20] (triangle).

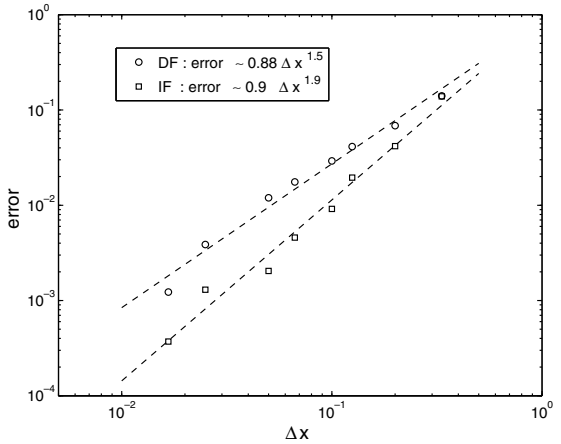

Fig. 4. Convergence of the drag coefficient computed with the IF (square) and the DF (circle). Dashed lines are exponential fits.

when using the DF and the IF. We observe that the IF is almost second-order by exhibiting a 1.9 exponent, whereas the DF shows an exponent of 1.5 when considering as an error measure the drag coefficient.

3.3. Flow at a moderate Reynolds number Re = 550

In a second impulsively started configuration, we increase the Reynolds number to $Re = 550$. The geometry of the system is chosen to match the one chosen in [22] and is of size $60D \times 34D$ with the cylinder centered around the point $(20D,17D)$ and the diameter $D = 160$. Fig. 5 shows the evolution of the velocity along the flow axis behind the cylinder at different times T. Simulation results compare well with experiments by Bouard and Coutanceau [4] and especially with LB simulations by Li et al. [22]. We however observe at $T = 1$ a slight departure close to cylinder when using the IF. We measure a maximum and normalized difference between DF and IF results of 4.3% at $T = 1$.

Fig. 6 shows the time evolution of the recirculation length L along the axis of the flow using the two forcing approaches. From time $T = 2$ there is excellent agreement between the present simulations and [22]. Similarly to what occurs when comparing velocities, the evolution of L differs at early times when

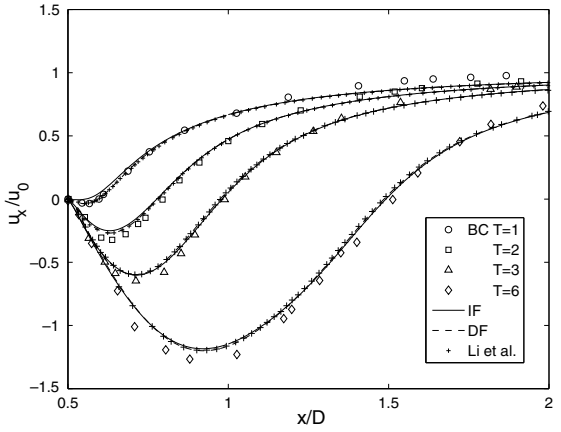

Fig. 5. Distribution of the x-velocity at different times T along the flow axis and behind an impulsively started cylinder at $Re = 550$. Results using the IF (solid line) and the DF (dashed line) are compared to experiments [4] (various symbols), and to simulation results from [22] (plus).

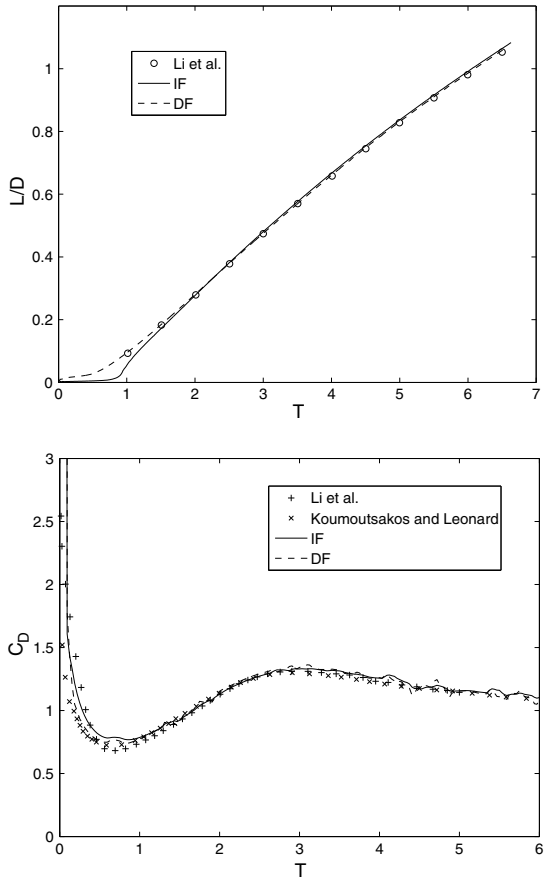

Fig. 6. Evolution of (top) the recirculation length and (bottom) of the drag coefficient on the flow axis behind an impulsively started cylinder at $Re = 550$. Results using the IF (solid line) and the DF (dashed line) are compared to simulations by Li et al. [22] (plus) and Koumoutsakos and Leonard [20] (cross).

using the IF. The time evolution of the drag coefficient is plotted in Fig. 6. We observe a quantitative match between present simulation results as compared to simulations by Li et al. [22] and Koumoutsakos and Leonard [20].

Considering this moderate Reynolds number, we observe that differences between flows computed using DF and IF are small as compared to differences obtained at $Re = 40$. This is due to the fact that the resolution needed to resolve all scales involved in the system is such that errors due to the boundary conditions are negligible at this resolution.

3.4. Vortex shedding of an impulsively started flow at Re = 200

We apply the present LB–IB method to the simulation of the periodic shedding of an impulsively started flow past a circular cylinder at Reynolds number $Re = 200$. The computational domain is $45D \times 20D$ with the cylinder of diameter $D = 40$ centered at $(15D, 10D)$. We use this configuration to validate the method for simulations at earlier as well as longer times and assess the capabilities of the method in capturing bluff body flow characteristics such as the Strouhal frequency.

Figs. 7 and 8 display the vorticity and velocity fields at early times for the DF and IF variants. We note that the vorticity field is largely similar from both simulations but certain differences are evident near the stagnation points and the recirculation zone. The difference in the boundary treatment is most apparent around stagnation points. For DF, the vorticity in the attachment and separation regions remains quite smooth (see

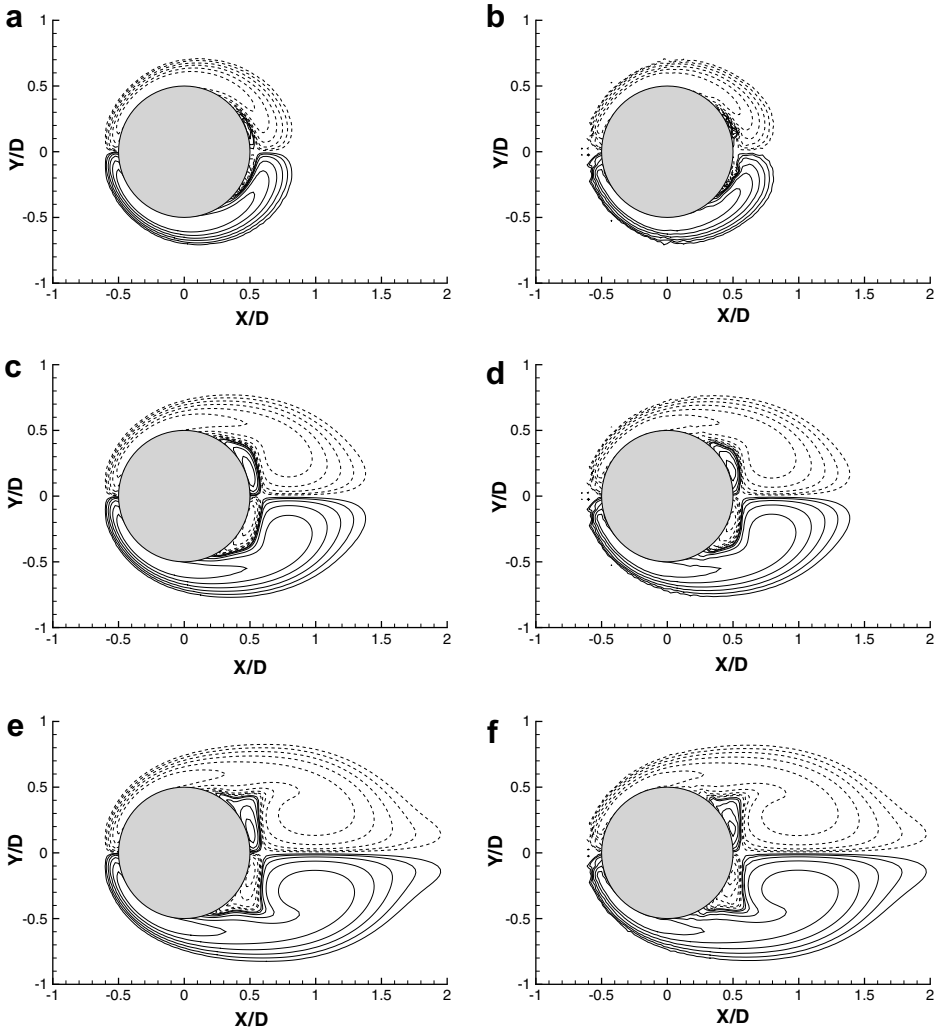

Fig. 7. Contours of vorticity past a cylinder at $Re = 200$ at early times. Contours corresponds to the values of $\omega D/u_0$: ± 0.25, 0.5, 1, 2, 4, 8 with the negative contours being dashed. (a) DF, $T = 1$, (b) IF, $T = 1$, (c) DF, $T = 3$, (d) IF, $T = 3$, (e) DF, $T = 5$, (f) IF, $T = 5$.

Fig. 7a, c and e) and the limiting streamline (originating at $Y = 0$ in Figs. 8a, c and e) always shows some deflection some distance above the wall. IF clearly displays a boundary layer developing more slowly near the front attachment point and some oscillations which are then carried downstream (see Figs. 7b, d and f). The same comment applies to the other stagnation points along the cylinder near the separation points and the reattachment region.

This behavior is expected as the stencil of IF does not smooth the forcing term and the lattice locations where it applies the x and y components of the forcing can present jumps(see Fig. 1).

To close this comparison, we remark that this difficulty, embodied by the double recirculation cell at $T = 1$(Fig. 8b), is most probably related to the slower circulation length growth already observed for the flow of Section 3.3 (Fig. 6).

The long time simulation leads to vortex shedding thus helping us assess the accuracy of the method when vortex structures interact with the downstream boundary conditions. Fig. 9 displays the vorticity field in the whole domain at the end of the simulation. The evolution of the force coefficient from the simulation using the IF approach (the DF results are almost indistinguishable) is shown in Fig. 10. The average value of the drag

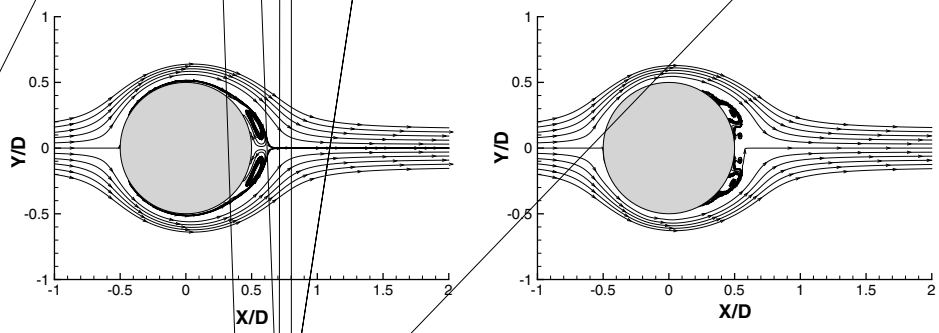

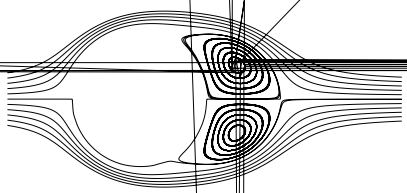

coefficient is 1.37, in good agreement with the study of Henderson [17] ($C_D = 1.36$). These force histories yield a Strouhal number $St = f\ u_0/D = 0.197$, in close agreement with related numerical (0.195 in Ref. [33]) and experimental results (0.196 in Ref. [36]).

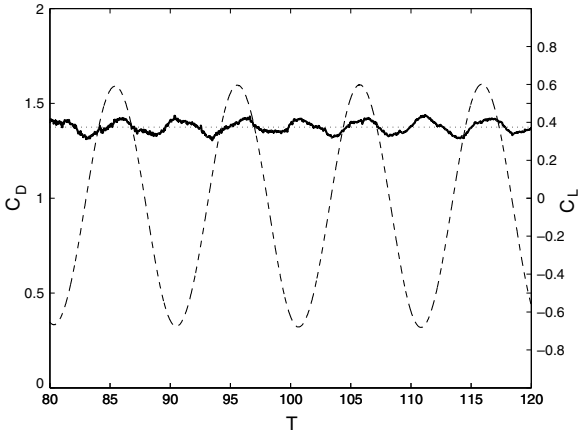

Fig. 10. History of force coefficients at $Re = 200$: C_D (solid line), average C_D (dotted) and C_L (dashed).

4. Conclusion

We present a novel method to couple a lattice-Boltzmann model of the Navier–Stokes equations with an immersed boundary method for the simulation of flows past complex boundaries. The present method relies on the simple incorporation of a forcing term in the LB model to enforce the no-slip boundary condition. The proposed LB–IB method has been validated with the simulation of the flow past an impulsively started cylinder at low and moderate Reynolds numbers. The simulation results are in good agreement with available experimental results and related benchmark computations. We remark that the present method has a straightforward implementation and allows for a direct computation of the forces experienced by the body.

We have examined two alternative approaches to exchange information between the boundary and the grid nodes, namely the interpolating forcing (IF) and the direct forcing (DF) approach. We note that the IF can handle implicit surface representations, making it suitable for level set representations that facilitate simulations of flows past complex deforming boundaries as in the case of multiphase flows. The IF and the DF approach exhibit an order of accuracy of 1.9 and 1.5 respectively, when computing the asymptotic value of the drag coefficient of the flow past an impulsively started cylinder. The higher accuracy of the IF is attributed to its non-mollified representation of the boundary which at the same time results in spurious vortical structures near under resolved stagnation points and thin boundary layers.

Present work involves the extension of the method to three-dimensions for the simulations of biological flows past unsteady complex geometries.

References

[1] D.J. Acheson, Elementary Fluid Dynamics, Oxford University Press, 1990.
[2] C. Anderson, M. Reider, A high order explicit method for the computation of flow about a circular cylinder, J. Comput. Phys. 125 (1996) 207.
[3] R. Botnar, G. Rappitsch, M.B. Scheidegger, D. Liepsch, K. Perktold, P. Boesiger, Hemodynamics in the carotid artery bifurcation: a comparison between numerical simulations and in vitro MRI measurements, J. Biomech. 33 (2000) 137.
[4] R. Bouard, M. Coutanceau, The early stage of development of the wake behind an impulsively started cylinder for $40 < Re < 10^4$, J. Fluid Mech. 101 (1980) 583.
[5] J.R. Cebral, R. Lohner, Efficient simulation of blood flow past complex endovascular devices using an adaptive embedding technique, IEEE Trans. Med. Image 24 (2005) 468.
[6] H. Chen, C. Teixeira, K. Molvig, Realization of fluid boundary conditions via discrete Boltzmann dynamics, Intl. J. Mod. Phys. C 9 (1998) 1281.
[7] B. Chopard, M. Droz, Cellular Automata Modeling of Physical Systems, Cambridge University Press, 1998.
[8] W. Collins, S. Dennis, Flow past an impulsively started circular cylinder, J. Fluid Mech. 60 (1973) 105.
[9] M. Coutanceau, R. Bouard, Experimental determination of the main features of the viscous flow in the wake of a circular cylinder in uniform translation. Part 1. Steady flows, J. Fluid Mech. 79 (1977) 231.

[10] M. Coutanceau, R. Bouard, Experimental determination of the main features of the viscous flow in the wake of a circular cylinder in uniform translation. Part 2. Unsteady flows, J. Fluid Mech. 79 (1977) 257.
[11] M.H. Dickinson, F.O. Lehmann, S.P. Sane, Wing rotation and the aerodynamic basis of insect flight, Science 284 (1999) 1954.
[12] A. Dupuis, B. Chopard, Theory and applications of an alternative lattice Boltzmann grid refinement algorithm, Phys. Rev. E 67 (2003) 066707.
[13] E.A. Fadlun, R. Verzicco, P. Orlandi, J. Mohd-Yusof, Combined immersed-boundary finite-difference methods for three-dimensional complex flow simulations, J. Comput. Phys. 161 (2000) 35.
[14] Z.-H. Feng, E.E. Michaelides, The immersed boundary-lattice Boltzmann method for solving fluid-particles interaction problems, J. Comput. Phys. 195 (2004) 602.
[15] Z.H. Feng, E.E. Michaelides, Proteus: a direct forcing method in the simulations of particulate flows, J. Comput. Phys. 202 (2005) 20.
[16] Z. Guo, C. Zheng, B. Shi, Discrete lattice effects on the forcing term in the lattice Boltzmann method, Phys. Rev. E 65 (2002) 046308.
[17] R.D. Henderson, Details of the drag curve near the onset of vortex shedding, Phys. Fluids 9 (1995) 2102.
[18] Y. Hoi, S.H. Woodward, M. Kim, D.B. Taulbee, H. Meng, Validation of CFD simulations of cerebral aneurysms with implication of geometric variations, J. Biomech. Eng. – Trans. ASME 128 (2006) 844.
[19] N.K.R. Kevlahan, O.V. Vasilyev, An adaptive wavelet collocation method for fluid–structure interaction at high Reynolds numbers, SIAM J. Sci. Comp. 26 (2005) 1894.
[20] P. Koumoutsakos, A. Leonard, High-resolution simulations of the flow around an impulsively started cylinder using vortex methods, J. Fluid Mech. 296 (1995) 1.
[21] J. Latt, B. Chopard, Lattice Boltzmann method with regularized pre-collision distribution functions, Math. Comp. Sim. 72 (2006) 165.
[22] Y. Li, R. Shock, R. Zhang, H. Chen, Numerical study of flow past an impulsively started cylinder by the lattice Boltzmann method, J. Fluid Mech. 519 (2004) 273.
[23] D.J. Mavriplis, Unstructured grid techniques, Ann. Rev. Fluid Mech. 29 (1997) 473.
[24] R. Mittal, G. Iaccarino, Immersed boundary methods, Ann. Rev. Fluid Mech. 37 (2005) 239.
[25] J. Mohd-Yusof, Combined immersed boundaries/B-splines methods for simulations geometries, CTR Ann. Research Briefs, NASA Ames, Stanford University, 1997.
[26] P. Moin, S.V. Apte, Large-eddy simulation of realistic gas turbine combustors, AIAA J. 44 (2006) 698.
[27] Y. Peng, C. Shu, Y.T. Chew, X.D. Niu, X.Y. Lu, Application of multi-block approach in the immersed boundary-lattice Boltzmann method for viscous fluid flows, J. Comput. Phys. 218 (2006) 460.
[28] C.S. Peskin, Numerical analysis of blood flow in the heart, J. Comput. Phys. 25 (1977) 220.
[29] C.S. Peskin, D.M. McQueen, Prosthetic heart-valves for numerical-analysis of blood flow in the heart, J. Comp. Phys. 37 (1980) 113.
[30] C.S. Peskin, The immersed boundary method, Acta Numer. 11 (2002) 479.
[31] S. Prakash, C.R. Ethier, Requirements for mesh resolution in 3D computational hemodynamics, J. Biomech. Eng. – Trans. ASME 123 (2001) 134.
[32] X. Shi, N. Phan-Thien, Distributed Lagrange multiplier/fictitious domain method in the framework of lattice Boltzmann method for fluid–structure interactions, J. Comput. Phys. 206 (2005) 81.
[33] S.P. Singh, S. Mittal, Flow past a cylinder: shear layer instability and drag crisis, Int. J. Numer. Method Fluids 47 (2005) 75.
[34] S. Succi, The Lattice Boltzmann Equation, For Fluid Dynamics and Beyond, Oxford University Press, 2001.
[35] M.S. Triantafyllou, G.S. Triantafyllou, D.K.P. Yue, Hydrodynamics of fishlike swimming, Ann. Rev. Fluid Mech. 32 (2000) 33.
[36] C.H.K. Williamson, 2-D and 3-D aspects of the wake of a cylinder, and their relation to wake computations, in: C.R. Anderson, C. Greengard (Eds.), Lectures in Applied Mathematics, vol. 28, American Mathematical Society, 1991.